CADERNOS UniFOA

Edição 54 | 2024 *e-ISSN: 1982-1816*

Data de submissão: 19/11/2023 Data de Aprovação: 03/06/2024

Modelo de análise estatística de uma célula de combustível de membrana de troca de próton

Statistical analysis model of a proton exchange membrane fuel cell

[1] Fábio José Bento Brum
[2] Thiago José Cyrne Moreno
[3] Weslley Luiz da Silva Assis

1 Universidade Federal Fluminense
2 Universidade Federal Fluminense
3 Universidade Federal Fluminense

RESUMO

A crescente preocupação com os impactos ambientais e o esgotamento das fontes de combustíveis fósseis o uso da tecnologia de células de combustível surge como uma alternativa. Essa tecnologia, que opera com gases de hidrogênio e oxigênio para produzir água e energia, destaca-se por sua capacidade de gerar energia sem emitir poluentes durante o processo. Este estudo aprofunda-se no funcionamento de uma célula de combustível de membrana polimérica, realizando uma análise estatística da influência das pressões dos reagentes e da temperatura de operação nas concentrações de reagentes na interface eletrodo-membrana, potencial de Nernst, e nas curvas de polarização e potência da célula. Para alcançar isso, foi utilizado um modelo comercialmente disponível de célula de combustível, conhecido como Ballard Mark IV, operando dentro de intervalos de pressão de 1 a 3 atm e temperaturas variando de 60 a 90°C. As concentrações de reagentes e o potencial de Nernst foram observados se aproximando de uma distribuição normal padronizada. Por outro lado, tanto a voltagem de saída da célula, quanto a potência elétrica desenvolvida, mostraram desvio do comportamento normalizado na região de efeitos de concentração. Modelos de regressão apresentaram um alto coeficiente de determinação, conferindo confiabilidade à formulação matemática. Condições operacionais ideais foram encontradas considerando a maximização da voltagem da célula, densidade de corrente, potência e eficiência. Neste estudo, a região de melhor eficiência da célula foi alcançada dentro de intervalos de pressão e temperatura de 2,5 a 3 atm e 78 a 90°C, respectivamente.

Palavras-chave:
célula Palavras-chave: célula de combustível; eficiência da célula; análise de distribuição de dados; modelos de regressão; projeto de experimentos.

ABSTRACT

The growing concern about environmental impacts and the depletion of fossil fuel sources has fueled research into new forms of energy derived from renewable sources. In this context, where the primary focus is on mitigating environmental pressures, the use of fuel cell technology appears as a way. This technology, which works on hydrogen and oxygen gases to produce water and energy, stands out for its capacity to generate power without emitting pollutants during the process. This study delves into the operation of a polymer membrane fuel cell, conducting a statistical analysis of the influence of reactant pressures and operating temperature on reactant concentrations at the electrode-membrane interface, Nernst potential, and the polarization and power curves of the cell. To achieve this, a commercially available fuel cell model, known as the Ballard Mark IV, was employed, working within pressure intervals of 1 to 3 atm and temperatures ranging from 60 to 90°C. The concentrations of reactants and Nernst potential were seen to approximate a standardized normal distribution. Conversely, the cell output voltage, as well as the developed electrical power, showed deviation from normalized behavior in the concentration effects region. Regression models proved a high coefficient of determination, thereby conferring reliability to the mathematical formulation. Optimal operational conditions were found by considering the maximization of cell voltage, current density, power, and efficiency. In this study, the region of best cell efficiency was reached within pressure and temperature ranges of 2.5 to 3 atm and 78 to 90°C, respectively.

Keywords:
fuel cell; cell efficiency; data distribution analysis; regression models; design of experiments.

1 INTRODUCTION

The fuel cell is an electrochemical device that converts chemical energy into electrical energy when supplied with gaseous hydrogen and an oxidizing agent, which can be either oxygen gas or atmospheric air (LOPES *et al*., 2013). Its operational principle is akin to batteries and cells, with the distinction that its reactants are stored externally to the devices and are continuously supplied. The chemical conversion occurs through the oxidation of hydrogen at the anode and the reduction of the oxidizing agent at the cathode, resulting in water vapor and energy as products of this reaction. In essence, it is a clean technology that does not emit polluting gases or compounds contributing to the greenhouse effect.

The reaction mechanism involves injecting hydrogen gas at the anode, where electrochemical reactions commence at the electrode/catalyst/electrolyte interface (LARMINIE e DICKS, 2003). Simultaneously, atmospheric air or oxygen is injected at the cathode. Ions formed at the anode interface pass through the electrolyte to the cathode, while electrons generated in the anode semi-reaction are transported through an external circuit to the cathode.

This study aims to contribute statistical models for predicting output variables based on crucial input variables of a polymer membrane cell, employing mathematical relationships derived from the data distribution of the analyzed parameters. The primary objective is to conduct a statistical analysis of the influence of operational variables such as hydrogen pressure, oxygen pressure, and operating temperature on output variables, including reactant concentrations, Nernst potential, cell voltage, electrical power, and fuel cell efficiency.

FUEL CELL MODEL

The model of the commercial cell mentioned by Leo *et al*. (2010) and validated in the algorithm proposed by Laviola (2017) establishes the Nernst potential by Equation 1 and reactant concentrations by Equations 2 and 3.

$$V_{Nernst} = 1{,}229 - 8{,}5*10^{-4}T(T-298{,}15) + 4{,}3085*10^{-5}(\ln(P_{H2}) + 1/2\ln(P_{O2})) \quad (1)$$

$$C_{H_2} = \frac{P_{H_2}}{1{,}09.10^6.e^{\left(\frac{77}{T}\right)}} \quad (2)$$

$$C_{O_2} = \frac{P_{O_2}}{5{,}08.10^6.e^{\left(\frac{-498}{T}\right)}} \quad (3)$$

The model asserts that the output voltage of the fuel cell can be measured by subtracting the reversible voltage from the internal losses of the device, as expressed in Equation 4.

$$Cell = Nernst - V_{ohm} - V_{ats} \quad (4)$$

As the V_{ohm} is recognized as the potential loss experienced by the electrical components of the cell, it can be represented by Equation 5 (LAVIOLA, 2017)

$$V_{ohm} = \Omega_1 \cdot j \cdot A + \Omega_2 \cdot T \cdot j \cdot A + \Omega_3 \cdot j_2 \cdot A_2 \quad (5)$$

Ω_1, Ω_2, and Ω_3 are parameters associated with ohmic losses and are presented in Table 1.

Table 1 - Ohmic Loss Coefficient

Coefficient	Value
Ω_1 (Ω)	-5,923157048805428x10^{-4}
Ω_2 (Ω/K)	-2,027378096297902x10^{-6}
Ω_3 (Ω/A)	-2,498597880151022x10^{-7}

Source: Laviola (2017)

Another factor influencing the cell's output voltage is the potential loss due to activation energy, which can be represented by Equation 6.

$$V_{ativ} = \xi 1 + \xi 2T + \xi 3Tln\,(A) + \xi 4Tln(C0_2) + \xi 5Tln(CH_2) + \xi 6Tln(jA) \quad (6)$$

Laviola (2017) developed a model where V_{ativ} in Equation 6 incorporates mass transport phenomena in the coefficients with indices 4 and 5. The coefficient values are defined in Table 2.

Table 2 - Activation Loss Coefficients

Coefficient	Value
ξ1 (V)	- 0,9440000
ξ2(V/K)	0,0028600
ξ3 (V/Kcm²)	0,0001970
ξ4 (V/Kmol)	0,0000430
ξ5 (V/Kmol)	0,0000780
ξ6 (V/KA)	- 0,0001960

Source: Laviola (2017)

The determination of the output power of the hydrogen cell will be carried out using Equation 7 (Laviola, 2017).

$$P = n_{cell} \cdot V_{cell} \cdot j \cdot A \quad (7)$$

2 STATISTICAL ANALYSIS OF THE CELL

The commercial fuel cell, recognized as the Ballard Mark IV, served as the reference model for this study (AMPHLETT, J.C *et al*, 1995). Leo *et al* (2010) details a fuel cell stack of this model with a membrane area of 232 cm² and a cell count of 1435. Laviola (2017) developed a computational algorithm extracting variables such as reactant concentration, Nernst potential, output voltage, and electrical power from reactant pressures and operating temperature in this commercial cell model. The values obtained from the computational program closely align with experimental behavior, showing an average error of 0.01%. The method employed in this study addresses the cell investigated by Leo *et al* (2010) using the magnitude values estimated by Laviola's algorithm (2017). To achieve this, an analysis table was structured simulating various operational conditions for the cell. The pressure variable was considered in the range of 1 to 3 atm and the operating temperature variable was within the range of 60 to 90°C.

Upon data consolidation, statistical tools such as normality testing, linear regression, quadratic regression, and the design of experiments were applied. The software tools Excel and Minitab were used to predict dependable statistical models concerning the behavior of the output variables proposed in this

study and found the best cell operating configuration. The statistical approach is Illustrated in Flowchart 1 in Figure 1.

Figure 1 – Statistical Analysis Flowchart

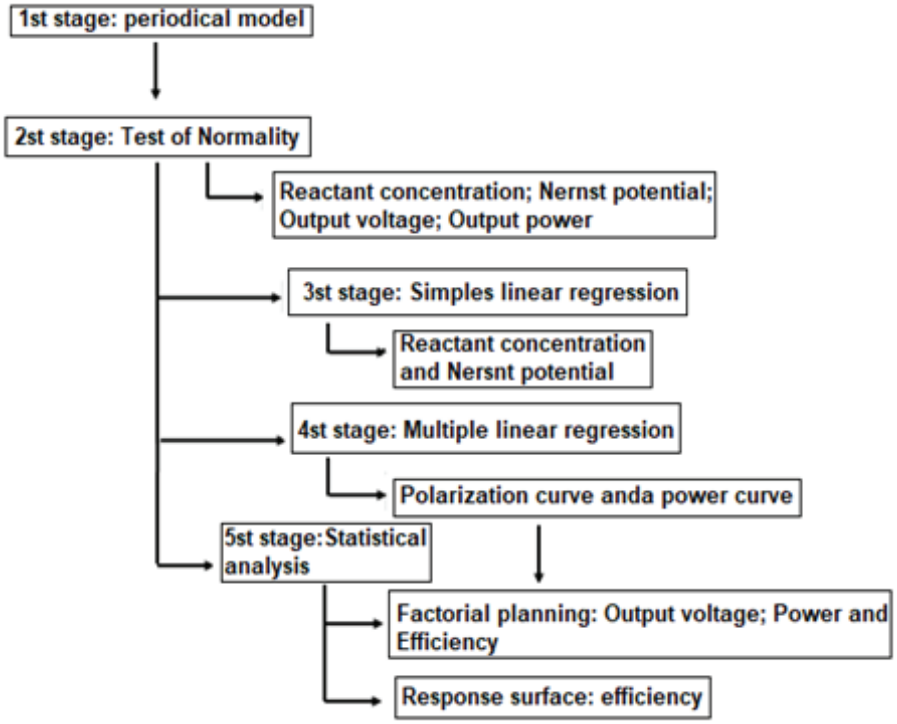

The authors (2024)

The normality test will be conducted using the Anderson-Darling function, as indicated in Equation 8 (BPI CONSULTING, 2011).

$$AD = -n - \frac{1}{n}\sum_{i=1}^{n}(2i-1)[lnF(xi) + ln\ ln\left(1 - F(x_{n-i+1})\right)] \quad (8)$$

Where n stands for the sample size, I denote the value of the analyzed parameter from an ascending order of data, and F (X_i) is a cumulative normal distribution function shown in Equation 9.

$$f(x) = 1 / (2\pi\sigma)^{1}/^{2}\ exp\ [-(x - \mu)^{2}/2\sigma^{2}] \quad (9)$$

When the sample size is less than or equal to 200 elements, the equation above can be adapted using Equation 10, where the asterisk symbol corresponds to the test limited to this quantity of data.

$$AD^{*} = AD(1 + \frac{0{,}75}{n} + \frac{2{,}25}{n^{2}}) \quad (10)$$

The normality test can be related to the p-value statistic, which, when exceeding 0.05, writes down data normality at a 95% confidence level. The computational program calculates the p-value based on different normality test values, with the criteria outlined below.

$$AD* \geq 0{,}6;\ p = exp\,(1{,}2937 - 5{,}709(AD*) + 0{,}0186(AD*)^2)$$
$$0{,}34 < AD < 0{,}6;\ p = exp\,(0{,}9177 - 4{,}279(AD*) - 1{,}38(AD*)^2)$$
$$0{,}2 < AD < 0{,}34;\ p = 1 - exp\,(-8{,}318 + 42{,}796(AD*) - 59{,}938(AD*)^2)$$
$$AD \leq 0{,}2;\ p = 1 - exp\,(-13{,}436 + 101{,}14(AD*) - 223{,}73(AD*)^2)$$

The regression models will be based on the minimization of the error (residual) (BARBETLA *et al*., 2004). For this purpose, the method of least squares will be employed, which is a powerful and widely used regression analysis method that is not restricted to linear relationships only. The value corresponding to the sample coefficient can be calculated using Equation 11.

$$\beta_1 = \underline{y} - \beta_2 \underline{x} \tag{11}$$

The sample coefficient , standing for the slope of the line, can be expressed in Equation 12.

$$\beta_2 = \frac{\sum_{i=1}^{n} (xi - \underline{x})\,(yi - \underline{y})}{\sum_{i=1}^{n} (xi - \underline{x})^2} \tag{12}$$

The bars placed atop the dependent and independent variables denote their mean values calculated over the sample data. Meanwhile, the index i shows the value of the input and output variables determined for each observed value. The coefficient of determination for a simple regression is obtained through Equation 13, where is the estimated value of the output variable.

$$R^2 = \frac{\sum_{i=1}^{n} (\dot{y}\imath - \dot{\underline{y}})^2}{\sum_{i=1}^{n} (yi - \underline{y})^2} \tag{13}$$

The least squares estimators of coefficients for the multiple linear and quadratic regression models are obtained through matrix equation 14, where X stands for the matrix of levels for each independent variable, and Y stands for the response matrix of output variables (HU *et al*., 2004).

$$\beta = (X^T X)^{-1} X^T Y \tag{14}$$

The estimated output variable follows Equation 15.

$$Y = X.\beta + \varepsilon \tag{15}$$

The design of experiments will consist of the factorial planning 3k, and the response surface method represented through contour plots (FARQAD AL-HADEETHI *et al*., 2015). The statistical model for the factorial planning follows the same rule as multiple linear regression, meaning that Equations 14 and 15 are adhered to.

3 RESULTS AND DISCUSSION

In the normality test, it was observed that the reactant concentration values concerning pressure variation follow a normal distribution, as the p-value yields a result exceeding 0.05. It can be affirmed that the sample data deviate from the mean by two times the standard deviation, considering the treated confidence interval is 95%. The data dispersion indicates that 50% of the data points lie above the

mean, and the other 50% lie below the mean. It is noteworthy that the Anderson-Darling values are the same as those obtained in the hydrogen concentration analysis. This phenomenon occurs because the function is strongly influenced by the size of the analyzed sample, which, in this case, remains constant. Regarding oxygen concentration, it is observed that the standard deviation is higher compared to hydrogen concentration. This implies that the data vary more around the mean when compared to hydrogen concentration. For the analysis with pressure variation, a sample size of 21 was considered. The normality test information is presented in Table 3.

Table 3 - Normality Test for Reactant Concentrations (10^{-7} mol/cm^3)

Graph	Sample size	Mean	Std deviation	Anderson Darling	P-value
$C_{H_2}\ x\ P_{H_2}\ a\ 60°C$	21	14,56	4,517	0,23	0,778
$C_{H_2}\ x\ P_{H_2}\ a\ 80°C$		14,75	4,577	0,23	0,778
$C_{H_2}\ x\ P_{H_2}\ a\ 90°C$		14,84	4,604	0,23	0,778
$C_{O_2}\ x\ P_{O_2}\ a\ 60°C$	21	17,57	5,449	0,23	0,778
$C_{O_2}\ x\ P_{O_2}\ a\ 80°C$		16,14	5,007	0,23	0,778
$C_{O_2}\ x\ P_{O_2}\ a\ 90°C$		15,52	4,816	0,23	0,778

The authors (2024)

The regression models for reactant concentration as a function of pressure variation are depicted in Figures 2 and 3.

Figure 2: Hydrogen concentration vs. partial pressure of hydrogen (A) 60°C and (B) 90°C.

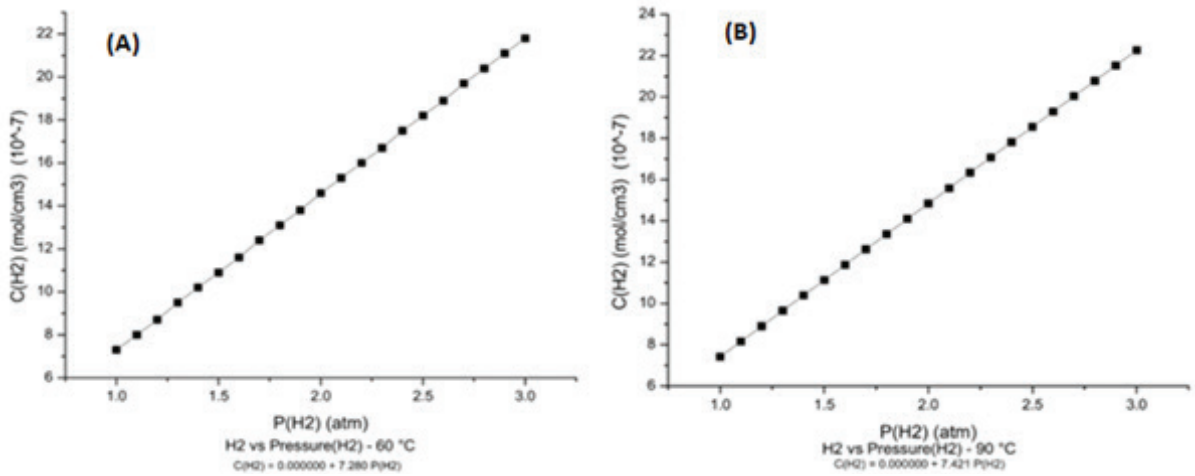

The authors (2024)

Figures 3: Oxygen concentration vs. oxygen partial pressure (A) 60°C and (B) 90°C.

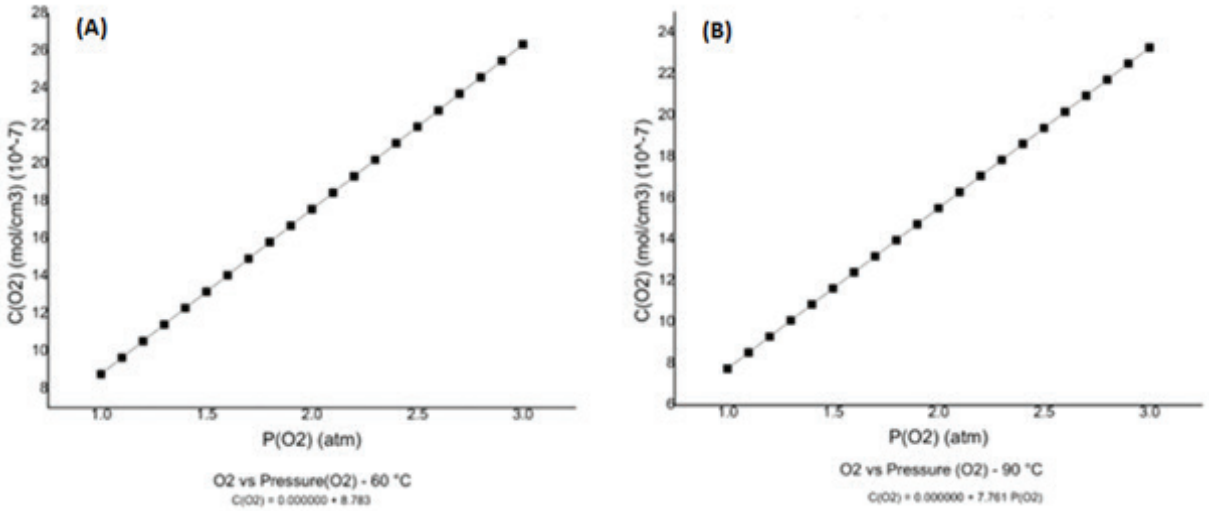

The authors (2024)

The analysis with pressure variation indicates that the angular coefficients of each linear regression exhibit values very close to each other. In other words, the simple act of increasing pressure does not significantly contribute to the increase in reactant concentration. For instance, hydrogen gas operates on the catalytic surface where the platinum catalyst is located. The reaction mechanism of molecular hydrogen occurs sequentially and depends on the availability of the catalytic site, which is related to the saturation of the catalyst (SILVA *et al*., 2017). On the other hand, the consumption of oxygen gas at the cathode depends on the arrival of hydroxide ions that traverse the polymer membrane after the dissociation of molecular hydrogen at the catalytic site.

The analysis of reactant concentration when the examined scenario involves temperature variation exhibits a larger dispersion around the mean concentration. In the case of reactant concentration with temperature variation, a sample size of 31 data points was considered. The normality test results are presented in Table 4.

Table 4 - Normality Test for Oxygen Concentration (10^{-7} mol/cm³)

Graph	Sample size	Mean	Std Deviation	Anderson Darling	P-value
$C_{H_2}\ x\ T a\ 1\ atm$	31	7,352	0,04256	0,334	0,49
$C_{H_2}\ x\ T\ a\ 2\ atm$		14,7	0,08511	0,334	0,49
$C_{H_2}\ x\ T\ a\ 3\ atm$		22,06	0,1277	0,334	0,49
$C_{O_2}\ x\ T\ a\ 1\ atm$	31	8,248	0,3091	0,343	0,467
$C_{O_2}\ x\ T\ a\ 2\ atm$		16,50	0,6182	0,343	0,467
$C_{O_2}\ x\ T\ a\ 3\ atm$		24,74	0,9274	0,343	0,467

The authors (2024)

It is seen that there was a decrease in the p-value compared to the analysis with pressure variation. This occurred due to the increase in the sample size. Nevertheless, it can still be asserted that the data follows a normalized distribution, as the obtained value is above the test statistic. It is noted that the

data dispersion was greater in the oxygen concentration. The regression curve analysis for the reactant concentration is presented in Figures 5 and 6.

Figures 5: Concentration of the reactants vs. temperature at 1 atm (atmosphere).

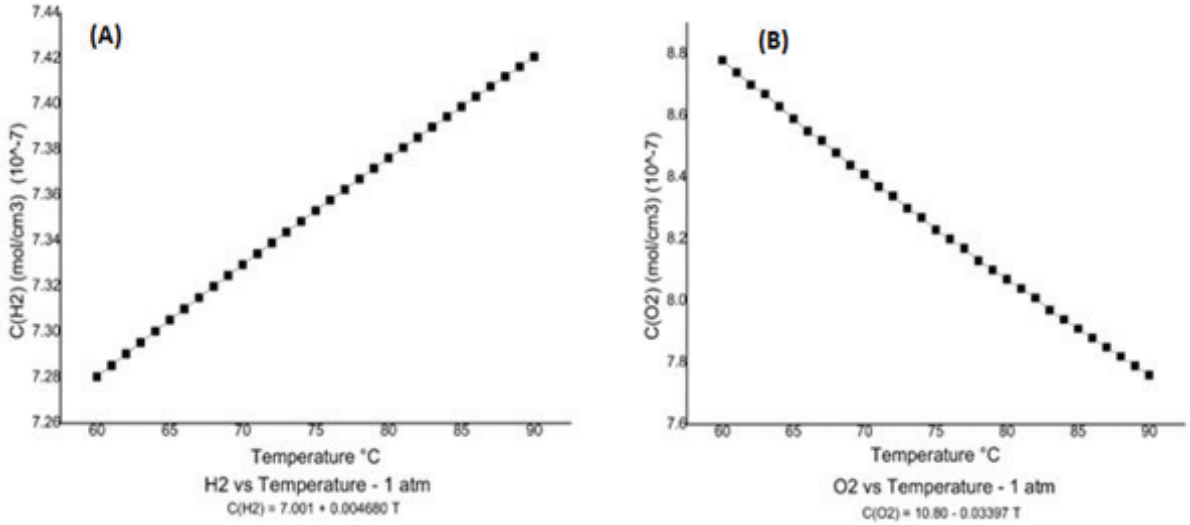

The authors (2024)

Figures 6: Concentration of the reactants vs. temperature at 3 atm (atmosphere).

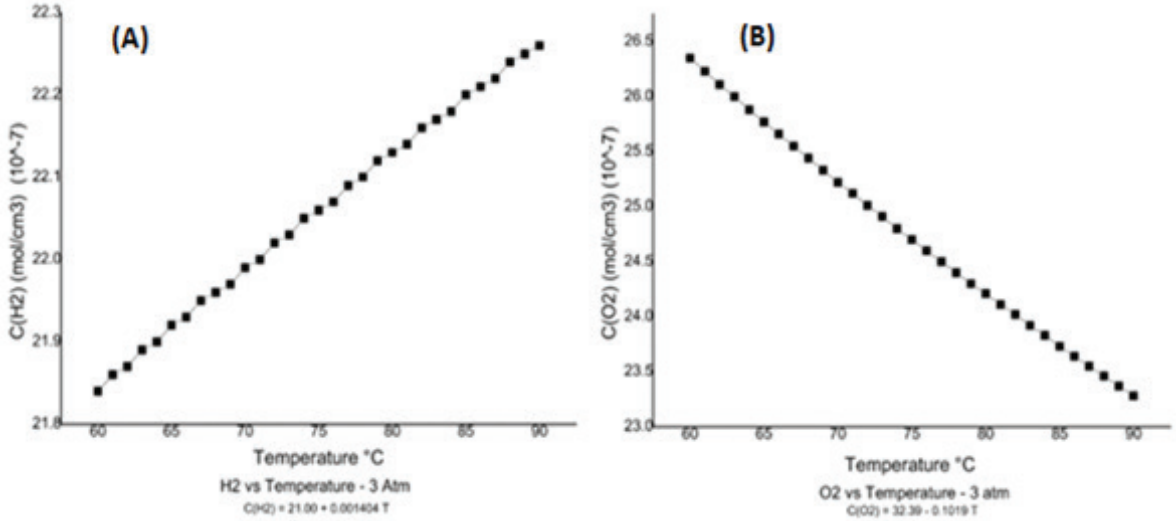

The authors (2024)

The angular coefficients of each linear regression exhibit different values. The line with a steeper incline, i.e., a higher angular coefficient, contributes to the increase in hydrogen concentration on the catalytic surface using a narrower temperature range, thereby reaching catalyst saturation at a lower operating temperature. The temperature increases with low reactant pressure - 1 atm may create a mismatch between hydrogen consumption and the arrival of this reactant at the catalytic layer. For oxygen concentration, the angular coefficient is negative, indicating a decreasing function (CAMPOS *et al*., 2018). This can be explained by the temperature increase favoring the arrival of hydroxide ions available

to reduce oxygen on the cathode side. The analysis of the average change in oxygen concentration per temperature interval follows the same interpretation as hydrogen concentration but with a decrease in the reactant. Understanding how oxygen gas behaves at the electrode-membrane interface is crucial, as an increase in concentration at the interface allows for an increased contact surface between oxygen molecules and hydroxide ions (MORENO *et al*., 2017).

After presenting the graphs of the data distribution related to the reactant gases, let's discuss the influence of pressure and temperature on the Nernst potential. The data distribution analysis for the Nernst potential with different pressure values is presented in Table 5, where the mean of the analyzed magnitude, standard deviation, sample size, and Anderson-Darling test will be verified.

Table 5 - Normality Test for Nernst Potential with Pressure Variation (Volts - V)

Graph	Sample size	Mean	Std Deviation	Anderson Darling	P-value
$V_{Nersnt}\ x\ P_{H_2}\ a\ 60°C$	21	1,216	0,004779	0,32	0,51
$V_{Nersnt}\ x\ P_{H_2}\ a\ 80°C$		1,20	0,05067	0,32	0,51
$V_{Nersnt}\ x\ P_{H_2}\ a\ 90°C$		1,192	0,005210	0,32	0,51
$V_{Nersnt}\ x\ P_{O_2}\ a\ 60°C$		1,218	0,002390	0,32	0,51
$V_{Nersnt}\ x\ P_{O_2}\ a\ 80°C$		1,203	0,002533	0,32	0,51
$V_{Nersnt}\ x\ P_{O_2}\ a\ 90°C$		1,195	0,002605	0,32	0,51

The authors (2024)

All previously mentioned characteristics of a normal curve are also reproduced for this analysis. The average result of the Nernst potential was close to the theoretical maximum potential in the analyses with pressure variation. The regression curves are presented in Figures 7 and 8.

Figure 7: Nernst Potential vs Hydrogen Pressure. (A) 60°C and (B) 90°C.

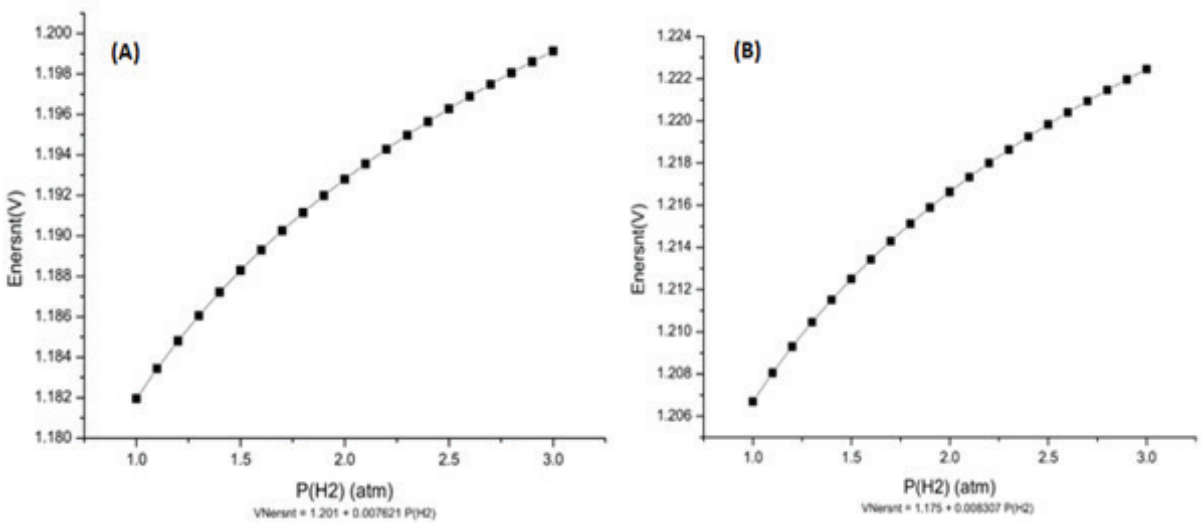

The authors (2024)

Figure 8: Nernst Potential vs. Oxygen Pressure. (A) 60°C and (B) 90°C.

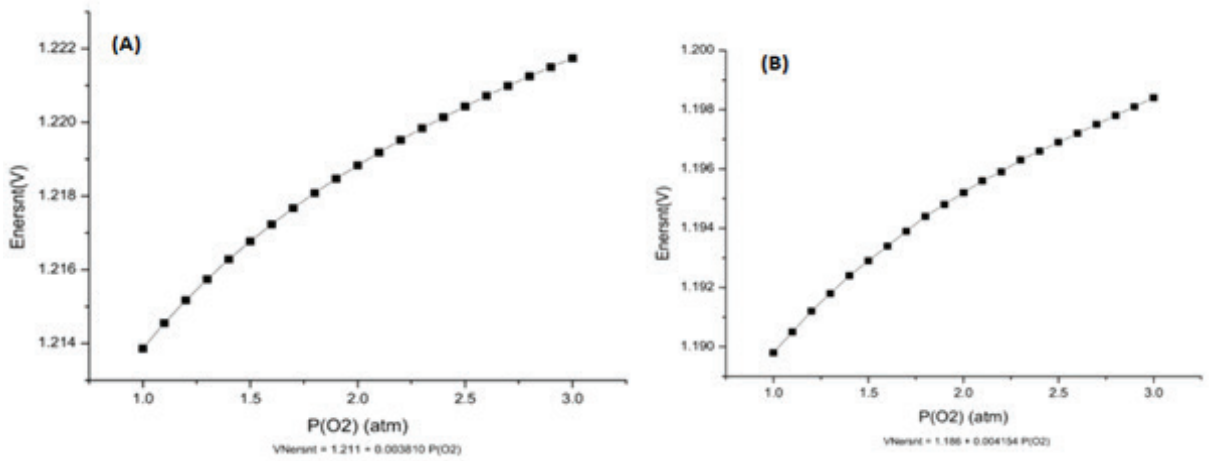

The authors (2024)

In general, both the increase in hydrogen partial pressure and oxygen partial pressure lead to a small increment in the open-circuit potential. However, this relationship should be managed with care because at higher temperatures, it will result in an increase in the amount of water produced on the cathode side, potentially causing blockages in the gas diffusion channels, hindering the arrival of reactants at the electrode-membrane interface, thus leading to a performance drop in the cell over time. The data distribution analysis for the open-circuit potential with different temperature values is presented in Table 6, where the mean of the analyzed magnitude, standard deviation, sample size, and Anderson-Darling test will be verified.

Table 6 – The normality test for the Nersnt potential varying the temperature.

Graphic	Mean	Std deviation	Anderson Darling	P-value
$ueV_{Nersnt}\ x\ T\ a\ 1\ atm$	1,187	0,007692	0,331	0,498
$V_{Nersnt}\ x\ T\ a\ 2\ atm$	1,202	0,007285	0,331	0,498
$V_{Nersnt}\ x\ T\ a\ 3\ atm$	1,212	0,007046	0,331	0,498

The authors, (2024)

The normality test for the variation of the Nernst potential with a change in temperature appears similarly to the Nernst potential with pressure variation. In Figures 9 and 10, the behavior of the open-circuit potential as a function of temperature with the same pressure value for hydrogen and oxygen is seen.

Figure 9: Nernst Potential vs. Temperature. (A) 1 atm and (B) 3 atm.

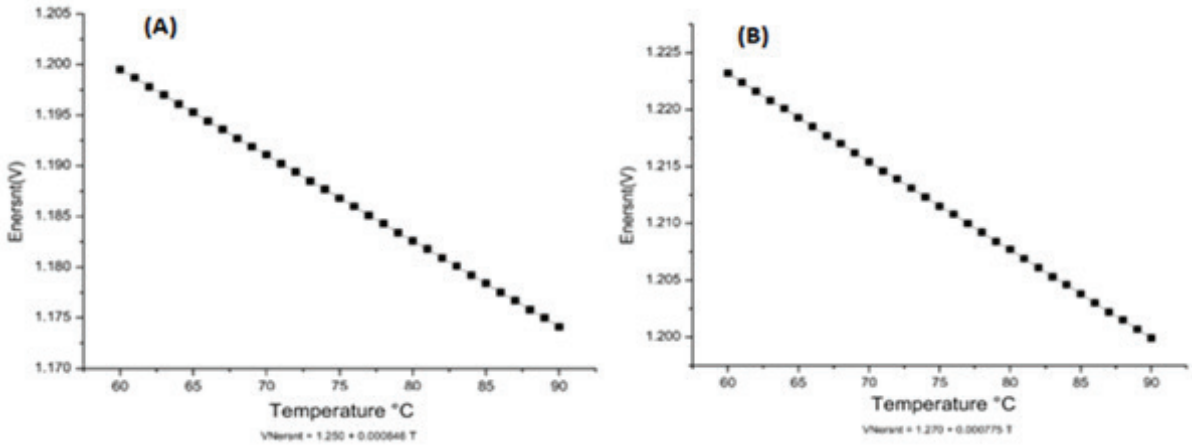

The authors (2024)

The thermodynamics of the cell and the open-circuit potential can be significantly affected by the operating temperature. Increasing the temperature will decrease the open-circuit potential. Temperature also influences proton conductivity and the passage of hydrogen through the membrane, as a temperature increase tends to be detrimental to the hydration of the polymer membrane. These effects are reflected in the overall performance of the fuel cell through the study of the polarization curve.

The characterization of a fuel cell is done through the polarization curve. This curve aims to relate the cell potential to the current density supplied by the cell, showing the points and effects that cause losses. Evaluating a typical polarization curve, we can highlight the main ranges with considerable losses related to activation, ohmic, and mass transport phenomena. The ohmic drop is represented in Figure 10.

Figure 10: Ohmic drop vs Current Density. (A) 1 atm and (B) 3 atm.

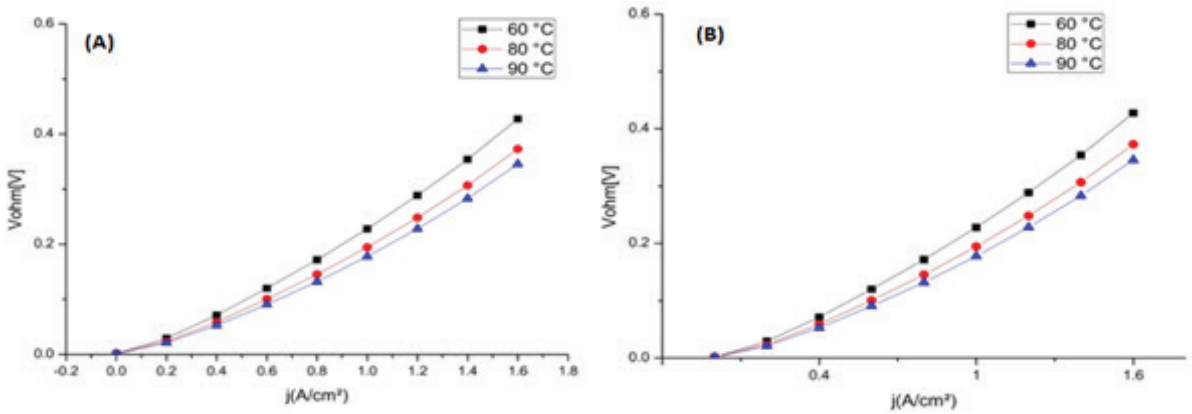

The authors (2024)

Pressure does not play a significant role in ohmic resistance with temperature being the determining factor in this phase. The performance improvement at higher temperatures is primarily due to the increased presence of protons in the membrane leading to an increase in its conductivity. However, an increase in temperature may lead to membrane dehydration, component degradation, and an increase in the hydrogen crossover rate due to the increased permeability coefficient of this element. Ohmic resistance plays a significant role in intermediate ranges of current density. The ohmic voltage values obtained for temperatures of 60°C, 80°C, and 90°C were 0.29 Ω.cm-2, 0.25 Ω.cm-2, and 0.24 Ω.cm-2, respectively. Resistance values are characterized by the slope of the line.

The other portion of loss is associated with activation polarization, which is related to the difficulty of the chemical reaction occurring due to the need to overcome an energy barrier between the reactants and the product. The behavior of this process under different pressure and temperature conditions is represented in Figure 11.

Figure 11: Voltage drop due to activation vs current density. (A) 1 atm and (B) 3 atm.

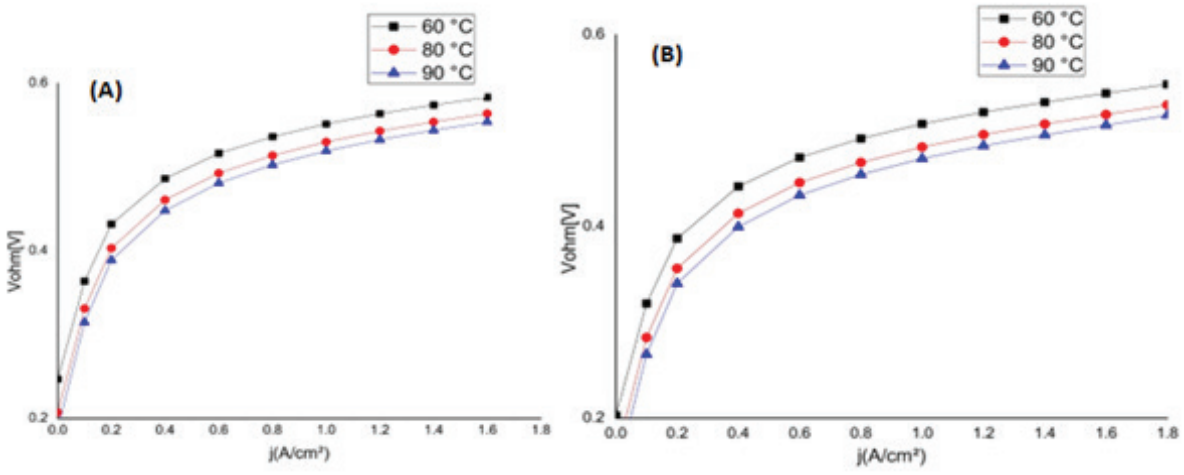

The authors (2024)

Graphical interpretation allows for verifying the operational situation that will lead to the best chemical kinetics condition. The lowest potential drop is represented by a partial pressure of 3 atm and an operating temperature of 90ºC. This occurs due to the greater availability of reactants in the gas diffusion channels and the increased probability of molecule collisions at a higher operating temperature. The role of the catalyst also equally influences the curves, as it is active in all conditions. Minimizing the drop due to polarization represents a relevant situation in the analysis because it is the most significant irreversible process in a fuel cell representing the major contribution to the voltage drop. In Laviola's formulation (2017), the concentration loss was considered one of the components of activation voltage.

The graph indicating the cell output voltage by the obtained current density is what the literature calls the polarization curve. Defining the cell voltage drop is of fundamental importance, as it allows for calculating the efficiency of the electrochemical device. A lower potential drop indicates better efficiency, i.e., the smaller the distance between the open-circuit potential and the polarization curve the better the cell efficiency.

The data distribution analysis for the cell output voltage with different pressure and temperature values is presented in Table 7, where the mean of the analyzed magnitude, standard deviation, sample size, and Anderson-Darling test will be verified.

Table 7 - Normality Test for Cell Output Voltage (Volts - V)

Graph	Sample size	Mean	Std deviation	Anderson Darling	P-value
V cell x j (1 atm/60°C)	200	0,4415	0,2069	1,091	0,007
V cell x j (1 atm/80°C)		0,4791	0,1922	1,008	0,011
V cell x j (1 atm/90°C)		0,4979	0,1849	0,971	0,014
V cell x j (2 atm/60°C)		0,4844	0,2069	1,091	0,007
V cell x j (2 atm/80°C)		0,5245	0,1922	1,008	0,011
V cell x j (2 atm/90°C)		0,5446	0,1849	0,971	0,014
V cell x j (3atm/60°C)		0,5094	0,2069	1,091	0,007
V cell x j (3 atm/80°C)		0,5511	0,1922	1,008	0,011
V cell x j (3 atm/90°C)		0,5719	0,1849	0,971	0,014

The authors (2024)

In the case of the polarization curve, it was observed that the output voltage data does not follow a normal distribution as the p-value is below 0.05. The Anderson-Darling test close to 1 indicates that the data of the analyzed magnitude are far from the perfect normal curve. The lack of normality in the data occurs in the region of concentration effects at low voltage and high current density. The polarization curves for different pressure and temperature conditions are represented in Figure 12.

Figure 12: Output voltage vs. current density. (A) 1 atm and (B) 3 atm.

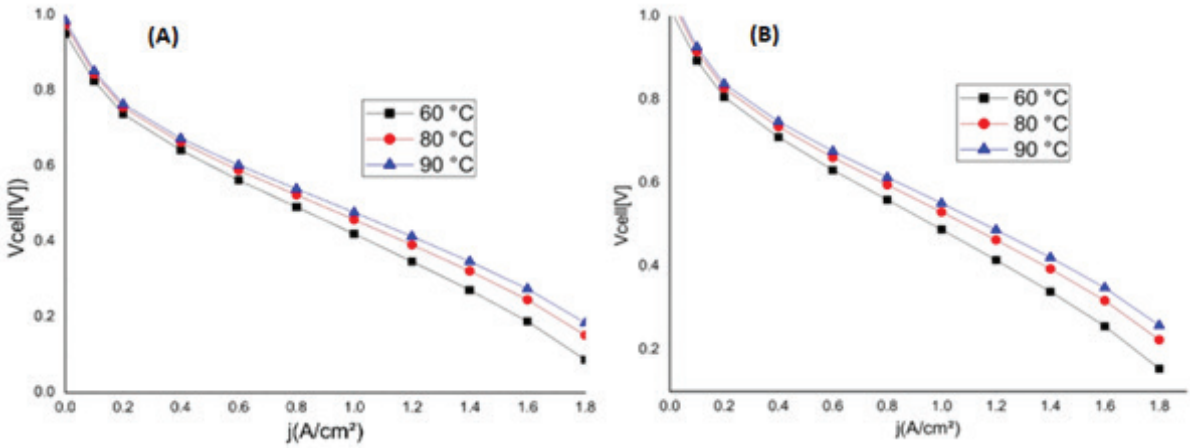

The authors (2024)

Through graphical analysis, it is observed that in the cases analyzed in this section, the best condition occurs when the operating temperature is 90°C and the pressure is 3 atm as it promotes the smallest slope of the curve concerning the Nernst potential.

The data distribution analysis for the power developed by the cell at different pressure and temperature values is presented in Table 8, where the mean of the analyzed magnitude, standard deviation, sample size, and Anderson-Darling test will be verified.

Table 8 - Normality Test for Cell Output Power (Kilowatt - kW)

Graph	Sample size	Mean	Std deviation	Anderson Darling	P-value
P cell x j (1 atm/60°C)	200	67,89	24,45	6,872	< 0,005
P cell x j (1 atm/80°C)		77,57	27,59	9,414	< 0,005
P cell x j (1 atm/90°C)		82,41	29,73	10,954	<0,005
P cell x j (2 atm/60°C)		76,88	27,17	8,080	< 0,005
P cell x j (2 atm/80°C)		87,10	31,52	11,128	< 0,005
P cell x j (2 atm/90°C)		92,21	34,25	12,128	<0,005
P cell x j (3 atm/60°C)		82,4	29,10	9,039	< 0,005
P cell x j (3 atm/80°C)		92,67	34,06	11,837	< 0,005
P cell x j (3 atm/90°C)		97,94	37,03	12,418	<0,005

The authors (2024)

The power data also does not follow a normal distribution as the p-value is below 0.05. The lack of normality occurred again in the cell concentration effect region. In this case, the Anderson-Darling test showed high values deviating significantly from a perfect normal curve. Figure 13 illustrates power as a function of current density under different pressure and temperature conditions.

Figure 13: Output Power vs Current Density. (A) 1 atm and (B) 3 atm.

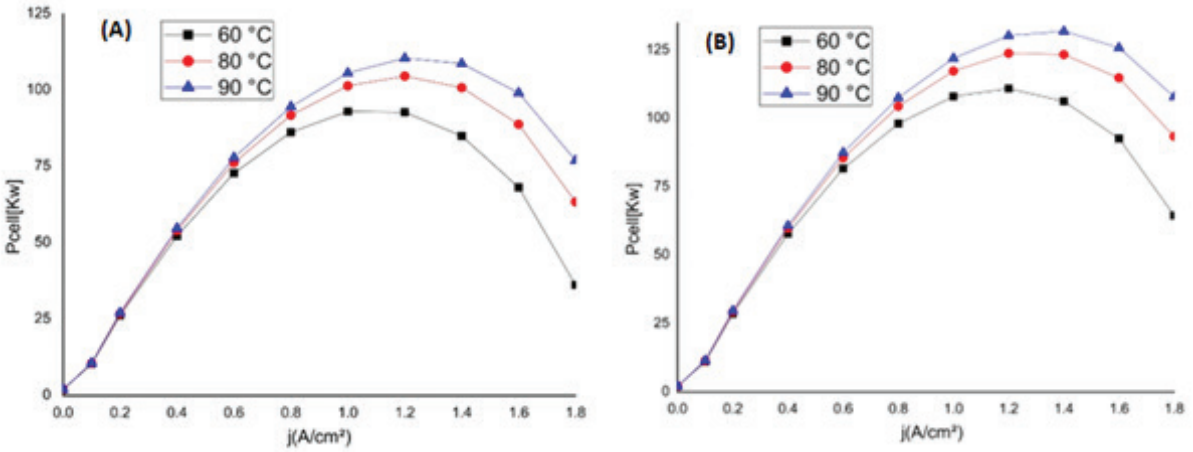

The authors (2024)

Through graphical analysis, it is observed that in the mentioned cases the best condition occurs with an operating temperature of 90°C as it promotes the steepest slope of the curve. The polarization curve and power developed by the cell show the best operational conditions through graphical analysis. However, such an approach is insufficient as it creates a restriction by not analyzing all possible pressure and temperature conditions and not discussing the cell efficiency. In order to make the analysis more comprehensive, a design of experiments is used through factorial planning and response surface methodology. The factorial design is represented in Figures 14, 15 and 16.

Figure 14: Interaction of Factors V

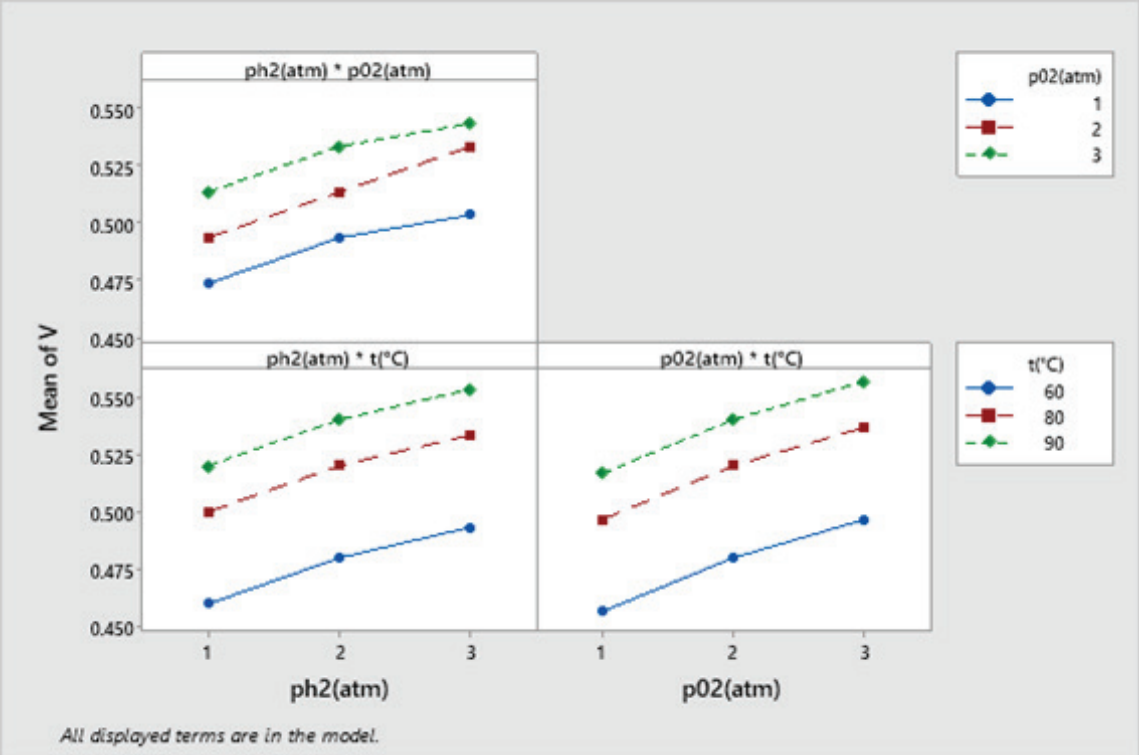

The authors (2024)

Figure 15: Interaction of Factors P

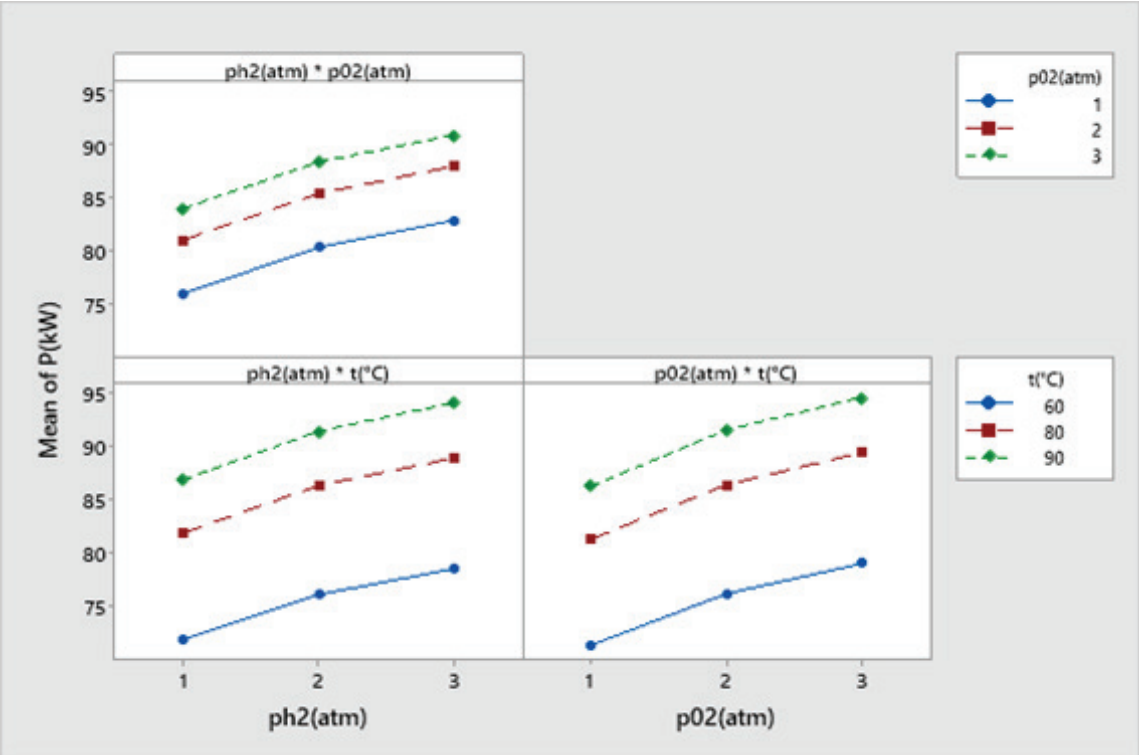

The authors (2024)

Figure 16: Efficiency Interaction

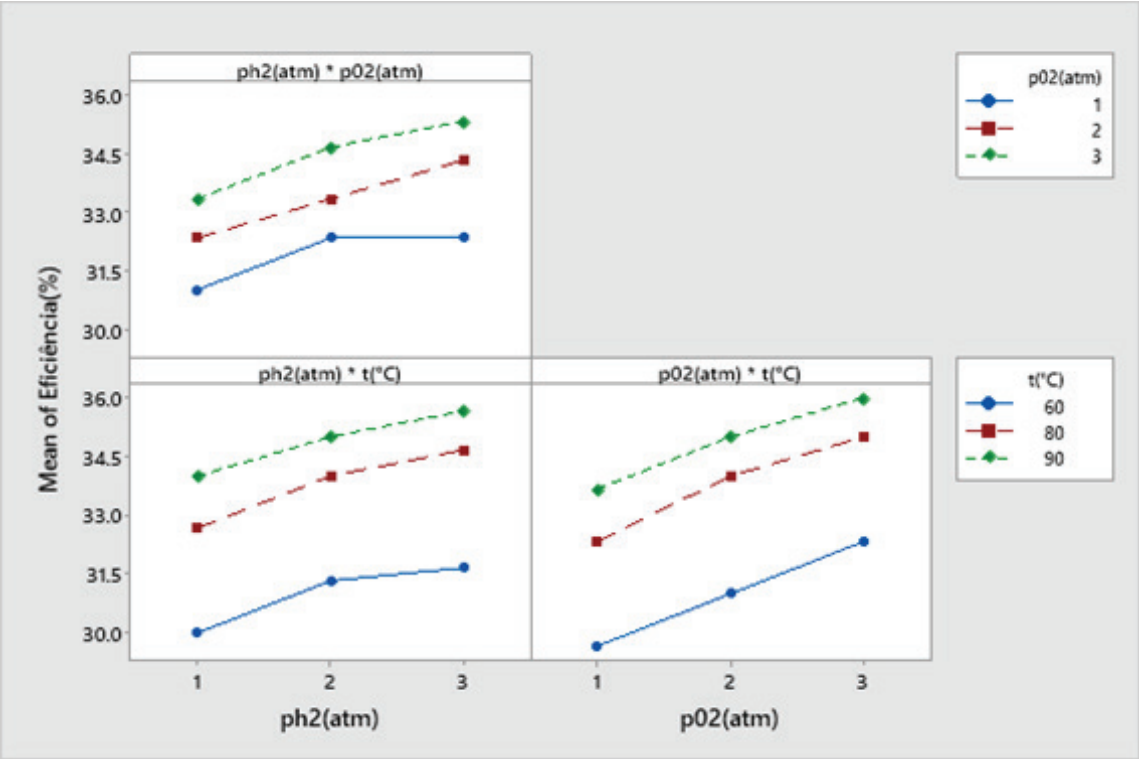

The authors (2024)

Observing the interactions of the operational variables, the best conditions that maximized voltage, power, and efficiency through factorial planning were at a pressure of 3 atm and an operating temperature of 90°C. Factorial planning uses an average value to represent the response variable and can predict the interactions between factors. The results align with the results obtained in the graphical analysis of the cell's polarization and power curve. This design of the experiment model works with fixed levels of factors, able to infer behavior through these benchmarks. To verify the efficiency behavior across the entire range of pressure and temperature values, response surfaces of efficiency are plotted in the contour plots of Figures 17, 18, and 19.

Figure 17: Efficiency (%) x PO_2(atm) x PH_2(atm)

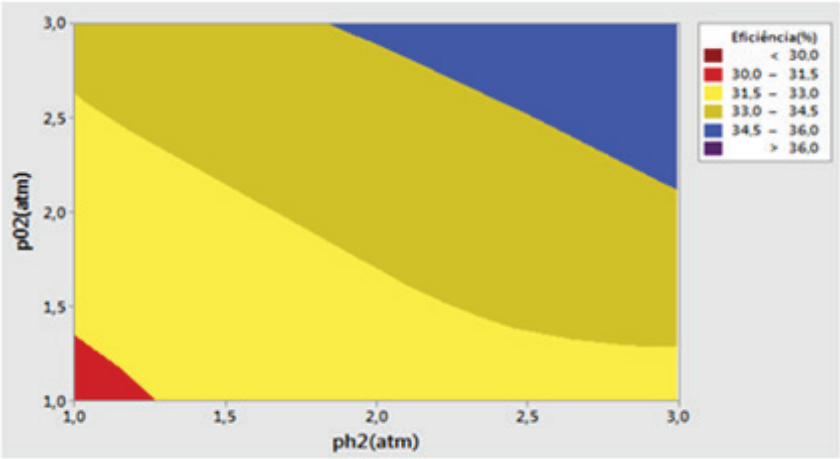

The authors (2024)

Figure 18: Efficiency (%) x T(°C) x PH_2 (atm)

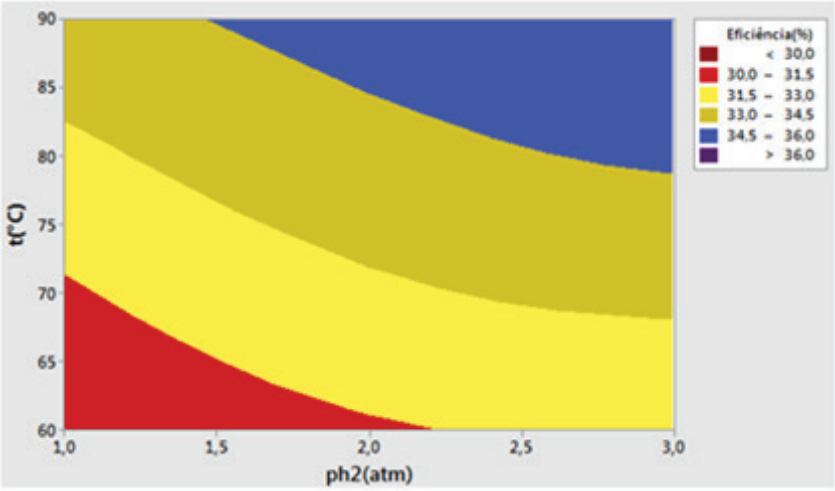

The authors (2024)

Figure 19: Efficiency (%) vs. Temperature (°C) vs. PO_2 (atm)

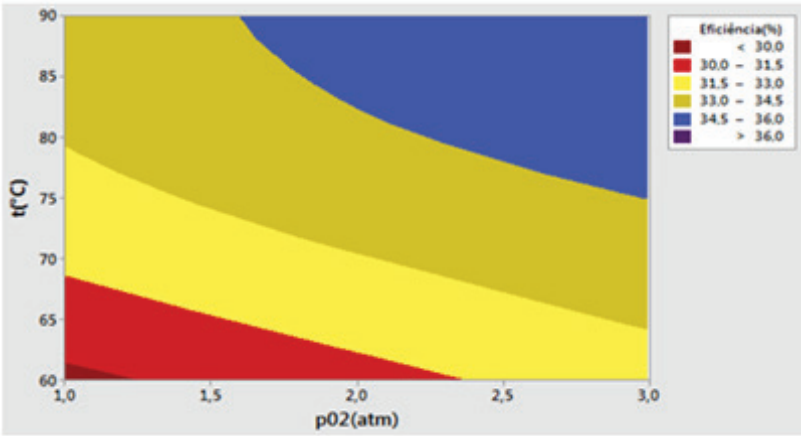

The authors (2024)

The level curves show that higher efficiency regions are more sensitive to variation of oxygen pressure from the temperature range of 75ºC. Temperatures below 70ºC and pressures below 1,5 atm indicate worse efficiency. When checking the contour points of the level curves it can be seen that the best efficiencies occur in the inferior limit of 2,5 atm of pressure and 78ºC and in the superior limit of 3 atm of pressure and 90ºC.

4 CONCLUSION

The use of statistical tools in fuel cells allows predicting the behavior of variables affecting the performance of this technology. In the commercial model Ballard Mark IV, the subject of this study, it was seen that the distribution of data for the variables of hydrogen concentration, oxygen concentration, and Nernst potential approached a standardized normal distribution with symmetric data around the mean, confirmed through the p-value parameter. However, the cell's output voltage and electrical power deviated from a normalized behavior in the concentration effects region. This occurred because the data in this region were outside the 95% confidence interval adopted as a criterion for statistical analysis.

The regression curves showed a good fit for the pressure and temperature intervals used reproducing with low residue the experimental cell used as a model for this work. The coefficient of determination denoted by R^2 ranged from 98% to 100%.

For hydrogen concentration, pressure variation played no significant role due to the sequential breaking of hydrogen molecules and their dependence on the ability of the platinum catalyst found in the active sites. An increase in temperature favored an increase in hydrogen concentration in the catalytic layer because of the higher kinetic energy of hydrogen molecules and a higher probability of collision, filling the platinum active sites more quickly.

Pressure variation for oxygen concentration also had no significant effect behaving similarly to hydrogen concentration under this operational parameter. On the other hand, an increase in temperature caused a decrease in oxygen at the electrode-membrane interface displaying a decreasing function in the statistical model. This is explained by more hydroxide ions reaching the cathode to react with the oxygen gas.

Regarding the Nernst potential, there was a decrease with an increase in temperature due to the higher water pressure in the system resulting in lower hydrogen and oxygen pressures. However, there was a slight increase in the Nernst potential with increasing pressure explained by the increased availability of reactants to perform the chemical reaction and produce electrical work.

In the polarization curves, regression models showed higher residue in the activation region. In the power curves, regression models showed higher residue in the concentration effects region. This dispersion can be explained because most of the sampled data belonged to the cell's ohmic region. Therefore, the regression model adjusted the equation to meet the broader sample range and reproduced the higher coefficient of determination.

Graphical analyses of polarization and power curves allow verification of cell efficiency through the least electrical potential drop aligned with maximum power. The statistical technique of design of experiments allows finding the best combination of operational variable values, within the established operation range in this work, to perfect voltage, current density, power, and efficiency parameters. For this dissertation, the region of the cell's best efficiency was achieved at pressure and temperature intervals of 2.5 to 3 atm and 78 to 90°C, respectively. The results for voltage, current density, power, and efficiency were seen to be 0.42 V, 1.215 A/cm², 119.72 kW, and 35% for 2.5 atm and 78°C, and 0.44 V, 1.296 A/cm², 132.17 kW, and 37% for 3 atm and 90°C. It was observed that the best condition always occurred in the ohmic region of the cell.

REFERENCES

AMPHLETT, J.C; BAURMERT R.M; MANN R.F; PEPPLEY B.A. *Performance modeling of the Ballard Mark IV solid polymer electrolyte fuel cell I. Mechanistic model development. Journal of the Electrochemical Society, v. 142, n. 1, p. 1-8, 1995.*

BARBETLA, REIS, BORNIA. *Estatística para Cursos de Engenharia e Informática*. Editora Atlas, 2004.

BPI CONSULTING. *Anderson-Darling test for normality*. 2011. Accessed online on 30 Sep 2018.

CAMPOS, C. F. B; ALMEIDA R. S; MORENO, T. J. C.; KORT L; SILVA, R. P; BRUM, F. J. B. Simulação Computacional do Escoamento de Hidrogênio para Diferentes Canais de Fluxo de uma Célula Combustível Tipo Membrana Polimérica. X Congresso Nacional de Engenharia Mecânica, 2018.

FARQAD AL-HADEETHI, MOH'D AL-NIMR, MOHMAMMAD AL-SAFADI. *Using the multiple regression analysis with respect to ANOVA and 3D mapping to model the actual performance of PEM (proton exchange membrane) fuel cell at various operating conditions. Energy. v 90, p. 475 -482, 2015.*

HU, G, FAN J, CHEN S, LIU Y. *Three-dimensional numerical analysis of proton exchange membrane fuel cells (PEMFCs) with conventional and interdigitated flow fields, Journal Power Sources, v. 136, p. 1-9, 2004.*

LARMINIE, J.; DICKS, A. *Fuel Cell Systems Explained. 2a ed. J. Wiley & Sons, New York, NY, EUA, 2003.*

LAVIOLA, Maximiller. *Avaliação energética e exergética em células combustíveis de membrana trocadora de prótons em regime permanente para diferentes variáveis de processo.* Dissertação de Mestrado. Universidade Federal Fluminense, 2017.

LEO, T. J.; DURANGO, J. A.; NAVARRO, E. *Exergy analysis of PEM fuel cells for marine applications. Energy, v. 35, n. 2, p. 1164-1171, 2010.*

LOPES, F. C., WATANABE, E. H., ROLIM, L. G. B., FURTADO, J. G. M., **"***Modelo Alternativo de um Empilhamento de Células a Combustível do tipo PEM Baseado em Rede Neural Recorrente para Aplicações de Controle em Tempo Real***"**. In: Anais do XXII Seminário Nacional de Produção e Transmissão de Energia Elétrica —XXII SNPTEE, Brasília-DF, Brasil, outubro 2013.

MORENO, T. J. C.; SILVA, R. P.; LAVIOLA, M.; CAMPOS, C. F. B; BRUM, F. J. B. *Influence of electrode flow channel changes on the Efficiency of Polymer Electrolyte Fuel Cell*. In: 24th ABCM International Congress of Mechanical Engineering, 2017, Curitiba. 24th ABCM International Congress of Mechanical Engineering, 2017.

SILVA, R. P.; MORENO, T. J. C; CAMPOS, C. F. B; BRUM, F. J. B. *Influence of the Modification of Anode a PEM Type Fuel Cell*. In: 24th ABCM International Congress of Mechanical Engineering, 2017, Curitiba. 24th ABCM International Congress of Mechanical Engineering, 2017.